SCIENTIFIC CULTURE

www.sci-cult.com

SCIENTIFIC CULTURE, Vol. 12, No. 4, (2026), pp. 11826-11841
Open Access. Online & Print

DOI: 10.5281/zenodo.20626429

HYDROGEOLOGICAL RISK ASSESSMENT OF PER- AND POLYFLUOROALKYL SUBSTANCES (PFAS) CONTAMINATION IN DRINKING WATER SOURCES: AN INTEGRATED FATE, TRANSPORT, AND MULTI-PATHWAY EXPOSURE FRAMEWORK

Sumbul Zafar[1], Munawwar Ali Khan[2]

[1]Research Scholar, Department of Geology, Aligarh Muslim University, Aligarh, Uttar Pradesh, India
[2]Research Scholar, Department of Civil Engineering, Birla Institute of Technology and Science (BITS), Pilani, Rajasthan, India
Email:ID: munawwar@gmx.us

Received: 04/04/2026
Accepted: 20/05/2026

ABSTRACT

Per- and polyfluoroalkyl substances (PFAS) are a new class of persistent organic contaminants that are emerging globally and have a wide range of toxicological properties, environmental persistence and fate and transport behaviour in saturated and unsaturated porous media, which makes them a serious threat to drinking water security. This study proposes a comprehensive, multi-module hydrogeological risk assessment framework that includes (i) aquifer characterisation and PFAS sorption geochemistry, (ii) one-dimensional advection-dispersion-reaction (ADR) transport modelling based on the Ogata-Banks analytical solution, (iii) multi-pathway human exposure assessment across ingestion, dermal contact, inhalation, and soil incidental ingestion routes, (iv) non-cancer hazard quotient (HQ) and hazard index (HI) calculations, (v) modified DRASTIC aquifer vulnerability indexing, and (vi) Monte Carlo probabilistic risk analysis (n = 10,000 iterations). Eight representative PFAS compounds were tested against current regulatory benchmarks such as the US EPA 2024 National Primary Drinking Water Regulation (NPDWR), WHO 2022 Guidelines, EFSA 2020 Tolerable Weekly Intake (TWI), and ATSDR Minimal Risk Levels. Results show that at a representative contaminated site (K = 1.5 m/d, foc = 1.2%, source C_0 = 500 µg/L), PFOA levels at a receptor well located 500 m away are 3,530 ng/L, which is 882 times higher than the US EPA MCL of 4 ng/L. The Deterministic Hazard Index (HI = 149.6) and EPA Mixture HI (26.1) are far above unity, indicating critical risk. The results of the Monte Carlo analysis show a P95 HQ of 2.8, and 78.3% of the simulations have HQ > 1

KEYWORDS: PFAS; groundwater contamination; fate and transport; advection-dispersion equation; hazard quotient; cancer risk; DRASTIC; Monte Carlo; drinking water; retardation factor; US EPA NPDWR 2024.

Copyright: © 2026. This is an open-access article distributed under the terms of the Creative Commons Attribution License. (https://cre-ativecommons.org/licenses/by/4.0/).

1. INTRODUCTION

Per- and polyfluoroalkyl substances (PFAS) comprise a structurally diverse family of more than 12,000 synthetic chemicals characterised by the presence of strong carbon-fluorine (C–F) bonds, conferring exceptional thermal, chemical, and biological stability (Buck et al., 2011; ITRC, 2020). First synthesised in the 1940s and commercially deployed from the 1950s onwards, PFAS were extensively used in fire-fighting aqueous film-forming foam (AFFF), non-stick coatings, food packaging, stain repellents, and industrial surfactants. Their ubiquitous environmental distribution and persistence have led to widespread detection in surface water, groundwater, soil, biota, and human serum across all continents, resulting in their designation as 'forever chemicals' (Cousins et al., 2022; Prevedouros et al., 2006). Groundwater represents the primary drinking water source for approximately 2.5 billion people globally (WHO, 2022). The hydrogeological pathways governing PFAS migration from point sources including AFFF-impacted military installations, industrial discharge zones, landfill leachate plumes, and wastewater irrigation areas to drinking water receptors are complex and compound-specific, governed by aquifer hydraulics, geochemical sorption, and physicochemical properties of individual PFAS congeners (Higgins & Luthy, 2006; Brusseau et al., 2020). Short-chain PFAS (C4–C6) exhibit significantly lower retardation factors relative to their long-chain homologues (C8+), resulting in faster and more extensive plume migration, whereas long-chain PFAS exhibit higher bioaccumulation potential and toxicity (Schaider et al., 2017).

The regulatory landscape governing PFAS in drinking water has undergone fundamental revision. The United States Environmental Protection Agency (US EPA) promulgated the first-ever National Primary Drinking Water Regulations (NPDWR) for PFAS in April 2024, establishing maximum contaminant levels (MCLs) of 4 ng/L for both PFOA and PFOS, and 10 ng/L for PFHxS, PFNA, and HFPO-DA (GenX), alongside a mixture Hazard Index (HI) requirement for six PFAS in combination (US EPA, 2024). The World Health Organization (WHO) 2022 Guidelines establish provisional guideline values of 100 ng/L for PFOA and PFOS individually, while the European Food Safety Authority (EFSA) recommends a group Tolerable Weekly Intake (TWI) of 4.4 ng/kg body weight per week for the sum of PFOA, PFOS, PFNA, and PFHxS (EFSA, 2020). The International Agency for Research on Cancer (IARC) classified PFOA and PFOS as Group 1 carcinogens (carcinogenic to humans) in 2023. Despite these regulatory advances, systematic quantitative frameworks integrating hydrogeological characterisation, multi-compound transport modelling, probabilistic exposure assessment, and uncertainty quantification remain scarce in the peer-reviewed literature, particularly for developing-country contexts where analytical capacity and site characterisation data are limited (Abunada et al., 2020; Ahrens & Bundschuh, 2014). Existing approaches frequently treat individual PFAS in isolation, omit uncertainty propagation, or decouple transport modelling from risk characterisation. This study addresses this gap by presenting an integrated, open-source Python-based framework encompassing all quantitative components of a Tier 2 PFAS risk assessment, from source characterisation to probabilistic receptor risk, validated against multiple international regulatory standards. The framework is designed to be modular, transparent, and reproducible, supporting application to diverse site conditions through parameterised uncertainty ranges informed by published field and laboratory data.

1.1 Objectives

The specific objectives of this study are: (1) to develop and validate an integrated hydrogeological–toxicological risk assessment framework for PFAS-impacted drinking water sources; (2) to quantify fate and transport of eight PFAS compounds using the Ogata-Banks (1961) analytical solution with retardation and first-order decay; (3) to perform multi-pathway exposure assessment for adult and child receptors via ingestion, dermal, inhalation, and soil pathways; (4) to compute Hazard Quotient, Hazard Index, ILCR, and EPA 2024 Mixture HI against current standards; (5) to characterise aquifer vulnerability using the modified DRASTIC index; and (6) to quantify parametric uncertainty through Monte Carlo simulation.

2. MATERIALS AND METHODS

2.1 Framework Architecture

The integrated framework comprises six sequential computational modules implemented in Python 3.12, utilising NumPy, SciPy, Pandas, and Matplotlib libraries. Figure 1 illustrates the conceptual site model linking source zones, subsurface transport pathways, and receptor exposure routes.

Appendix A: Dose-Response Relationships and Regulatory Isopleths

Figure A1 presents computed Hazard Quotient

(HQ) and Incremental Lifetime Cancer Risk (ILCR) as continuous functions of water concentration for PFOA and PFOS across six orders of magnitude, enabling rapid screening of measured field concentrations against risk thresholds without recourse to full calculation

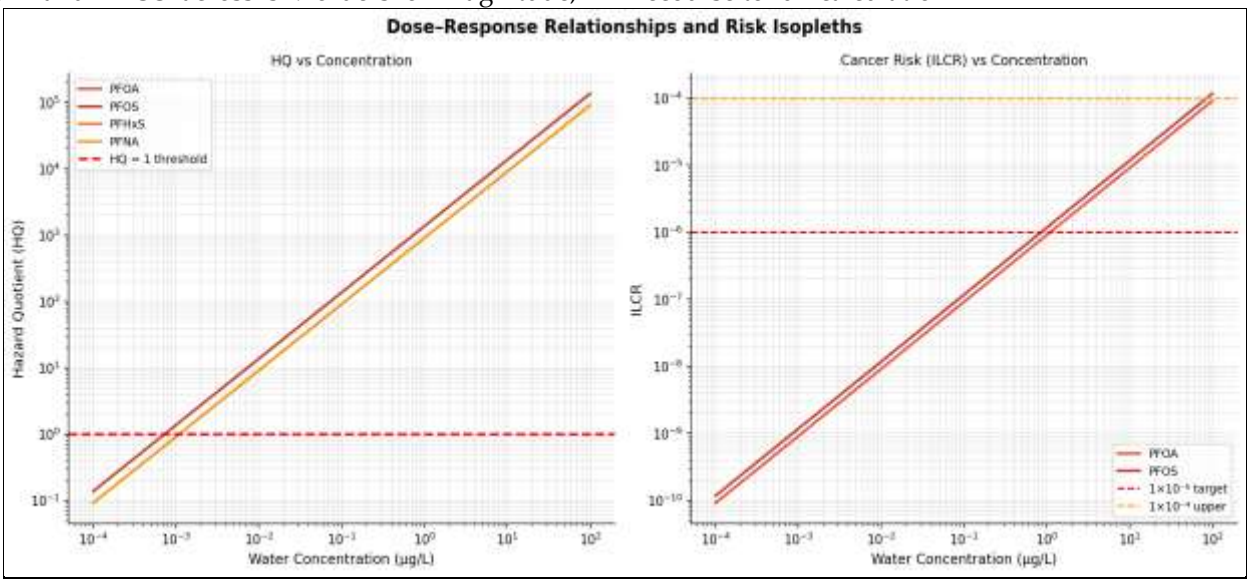


Figure A1. Dose-response relationships: (left) HQ as a function of water concentration (µg/L) for four PFAS compounds; (right) ILCR as a function of concentration for PFOA and PFOS. Red dashed lines indicate HQ = 1 and ILCR = 10^{-6}/10^{-4} benchmarks.

Appendix B: Executive Risk Summary Dashboard

Figure B1 provides an integrated executive dashboard consolidating all key risk metrics, plume profile, HQ/ILCR results, and Monte Carlo summary for rapid stakeholder communication.

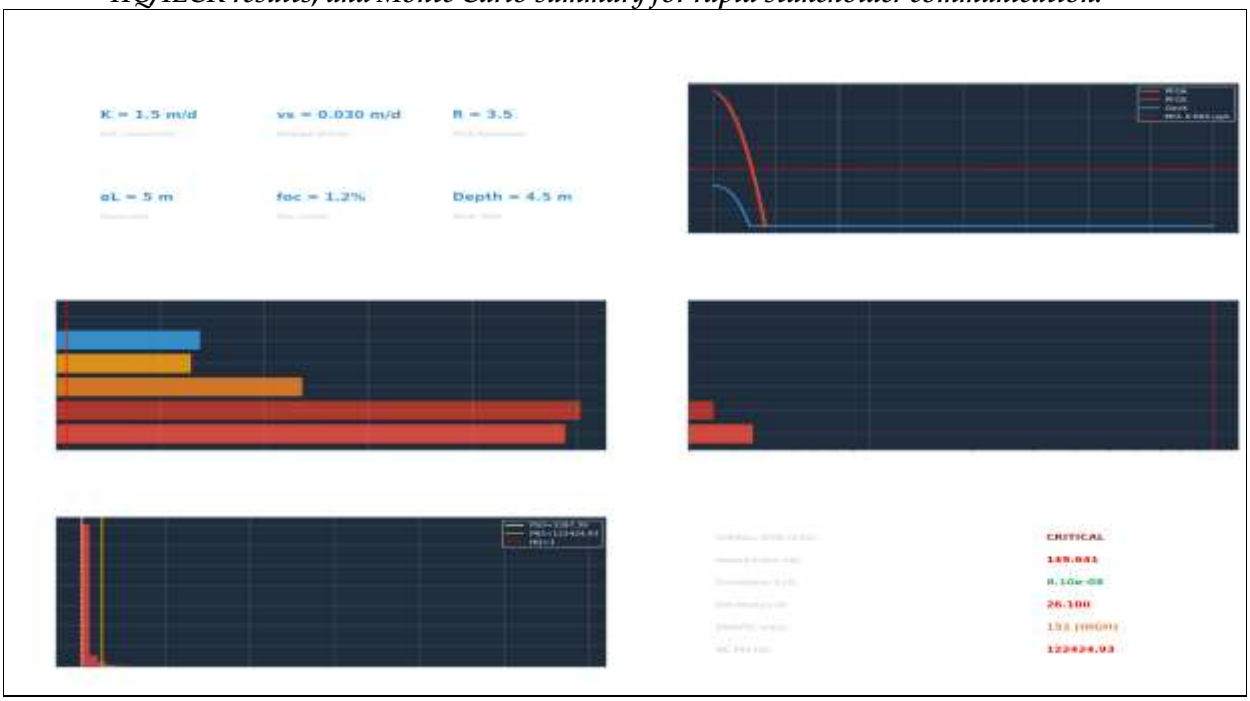


Figure B1. Executive risk summary dashboard: site parameters (top-left), plume profile (top-right), hazard quotients (middle-left), cancer risk (middle-right), Monte Carlo HQ distribution (bottom-left), and risk-level summary (bottom-right).

Appendix C: Multi-Property PFAS Radar Chart.

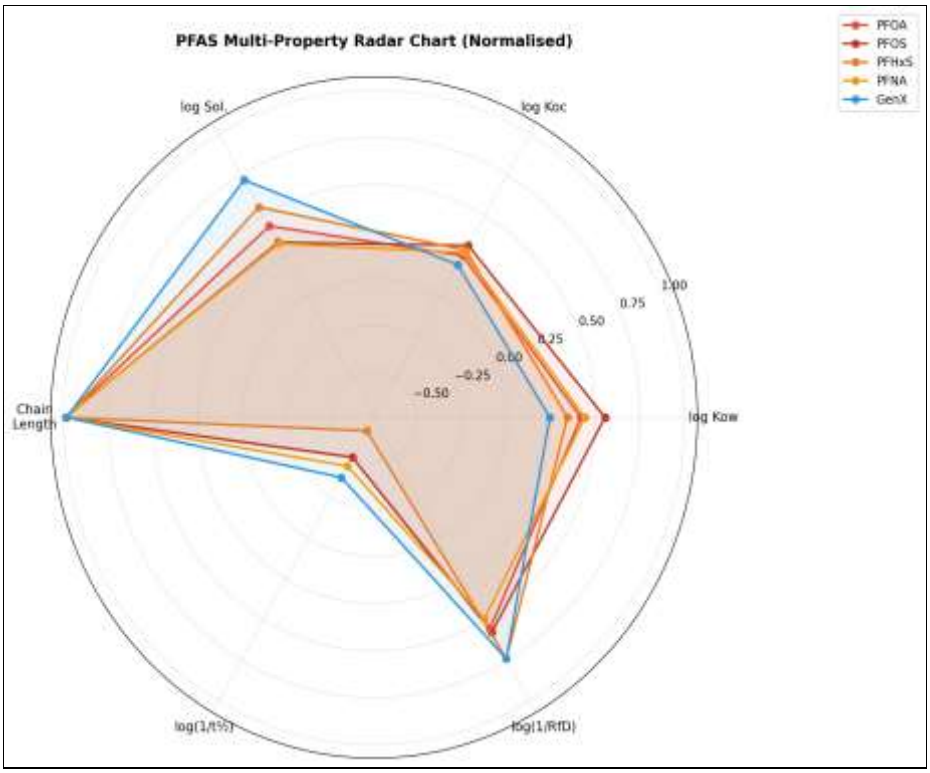


Figure C1. Normalised multi-property radar chart comparing PFOA, PFOS, PFHxS, PFNA, and GenX across six physicochemical properties (log Kow, log Koc, log solubility, chain length, persistence proxy, toxicity proxy).

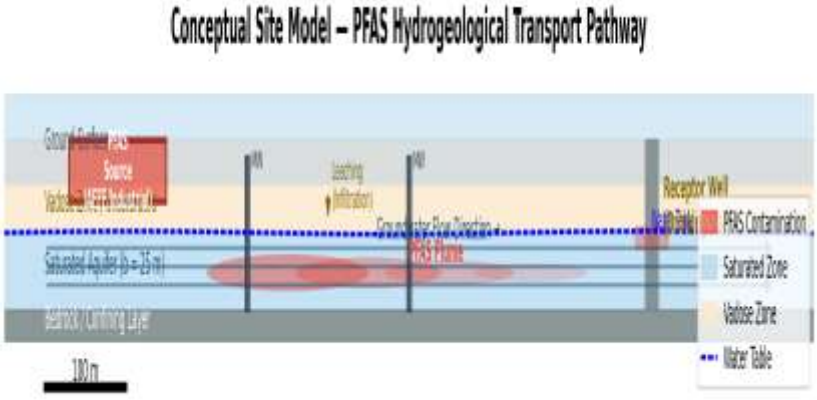


Figure 1. Conceptual site model illustrating PFAS source zones, vadose zone leaching, saturated aquifer transport via advection and dispersion, and drinking water well receptor. Modified after ITRC (2020).

2.2 Hydrogeological Characterisation

Site hydrogeological parameters were derived from standard aquifer testing and laboratory analysis procedures consistent with USGS and US EPA guidance (Domenico & Schwartz, 1998). The transmissivity (T, m²/d), seepage velocity (vs, m/d), and longitudinal hydrodynamic dispersion coefficient (DL, m²/d) were calculated as:

$$T = K \times b$$

$$vs = (K \times i) / ne$$

$$DL = \alpha L \times vs + \tau \times Dm$$

where K is hydraulic conductivity (m/d), b is saturated thickness (m), i is hydraulic gradient (m/m), ne is effective porosity (dimensionless), αL is longitudinal dispersivity (m), τ is tortuosity (≈ 0.7), and Dm is molecular diffusivity (m²/d). Transverse and vertical dispersivities were estimated as αT = αL/10 and αV = αL/100 (Gelhar et al., 1992). Default site parameters used in this study are summarised in Table 1.

Table 1. Hydrogeological site characterisation parameters used in the risk assessment framework.

Hydraulic Conductivity	K	m/d	1.5	Pumping test (USGS)
Saturated Thickness	b	m	25.0	Borehole logs
Transmissivity	T	m²/d	37.5	T = K × b
Effective Porosity	ne	—	0.25	Laboratory (ASTM D7263)
Hydraulic Gradient	i	m/m	0.005	Water table survey
Darcy Flux	q	m/d	0.0075	q = K × i
Seepage Velocity	vs	m/d	0.030	vs = K × i / ne
Bulk Density	ρb	g/cm³	1.65	Core analysis (ASTM D7263)
Fraction Organic Carbon	foc	g/g	0.012	TOC analysis (EPA 9060A)
Long. Dispersivity	αL	m	5.0	Gelhar et al. (1992)
Depth to Water Table	Dw	m	4.5	Monitoring well network
Source Concentration	C□	µg/L	500	Field sampling (EPA 537.1)

2.3 PFAS Physicochemical and Toxicological Properties

Eight PFAS compounds spanning perfluorocarboxylic acids (PFCAs) and perfluorosulfonic acids (PFSAs) of chain lengths C4–C10 were selected based on regulatory prioritisation, environmental prevalence, and availability of validated physicochemical parameters (Table 2). Organic carbon normalised partition coefficients (Koc) were sourced from Higgins and Luthy (2006) for long-chain PFAS and from ITRC (2020) for short-chain homologues. Reference doses (RfD) and cancer slope factors (CSF) were obtained from US EPA IRIS (2022) and ATSDR (2021).

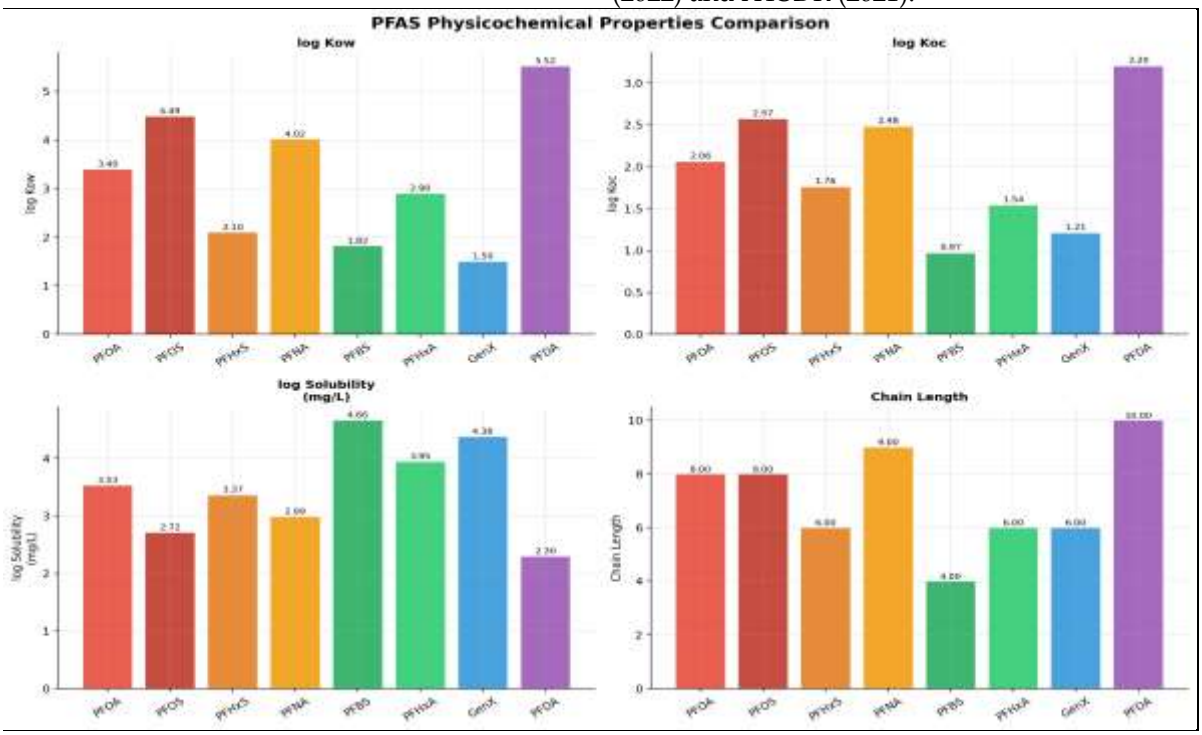


Figure 2. Comparison of key physicochemical properties of eight PFAS compounds: (a) log Kow, (b) log Koc, (c) log water solubility, and (d) carbon chain length. Data sources: Higgins & Luthy (2006), ITRC (2020), ATSDR (2021).

Table 2. Physicochemical and toxicological properties of target PFAS compounds.

PFOA	335-67-1	414.07	2.06	114.8	3×10□□	4	IARC Group 1
PFOS	1763-23-1	538.22	2.57	371.5	2×10□□	4	IARC Group 1
PFHxS	355-46-4	438.17	1.76	57.5	3×10□□	10	Group 2B
PFNA	375-95-1	464.08	2.48	301.9	3×10□□	10	Group 2B
PFBS	375-73-5	338.09	0.97	9.3	1.0	200	Inadequate data
PFHxA	307-24-4	314.05	1.54	34.7	6×10□³	None	Inadequate data
GenX (HFPO-DA)	13252-13-6	330.05	1.21	16.2	3×10□□	10	Possible
PFDA	335-76-2	514.08	3.20	1584.9	3×10□□	None	Possible

2.4 Fate and Transport Model

2.4.1 Retardation and Sorption

Linear equilibrium sorption was assumed, governed by a compound-specific distribution coefficient Kd (L/kg) derived from Koc and foc:

$$Kd = Koc \times foc \quad (1)$$

The retardation factor R quantifying reduced transport velocity relative to pore water flow is given by (Freeze & Cherry, 1979):

$$R = 1 + (\rho b \times Kd) / ne \quad (2)$$

The retarded seepage velocity is $vr = vs / R$ (m/d), and the retarded travel time to a receptor at distance x is $t = x \times R / vs$ (days).

2.4.2 Ogata-Banks Analytical Solution

One-dimensional transient PFAS transport in a homogeneous, isotropic confined aquifer was described by the advection-dispersion-reaction equation incorporating first-order decay ($\lambda = \ln(2)/t_{½}$, d^{-1}):

$$R \bullet \partial C/\partial t = DL \bullet \partial^2 C/\partial x^2 - vr \bullet \partial C/\partial x - \lambda \bullet C \quad (3)$$

The Ogata-Banks (1961) analytical solution was implemented with retardation and radioactive decay analogy:

$$C(x,t) = (C_0/2) \bullet [\mathrm{erfc}((x - vr \bullet t) / (2\sqrt{(DL \bullet t)})) + \exp(vr \bullet x/DL) \bullet \mathrm{erfc}((x + vr \bullet t) / (2\sqrt{(DL \bullet t)}))] \bullet \exp(-\lambda \bullet t) \quad (4)$$

For PFAS, first-order decay is negligible ($\lambda \approx 0$; half-lives > 27 years in groundwater), reducing Equation (4) to the standard Ogata-Banks form. Steady-state concentration profiles were evaluated for plume delineation and receptor impact assessment.

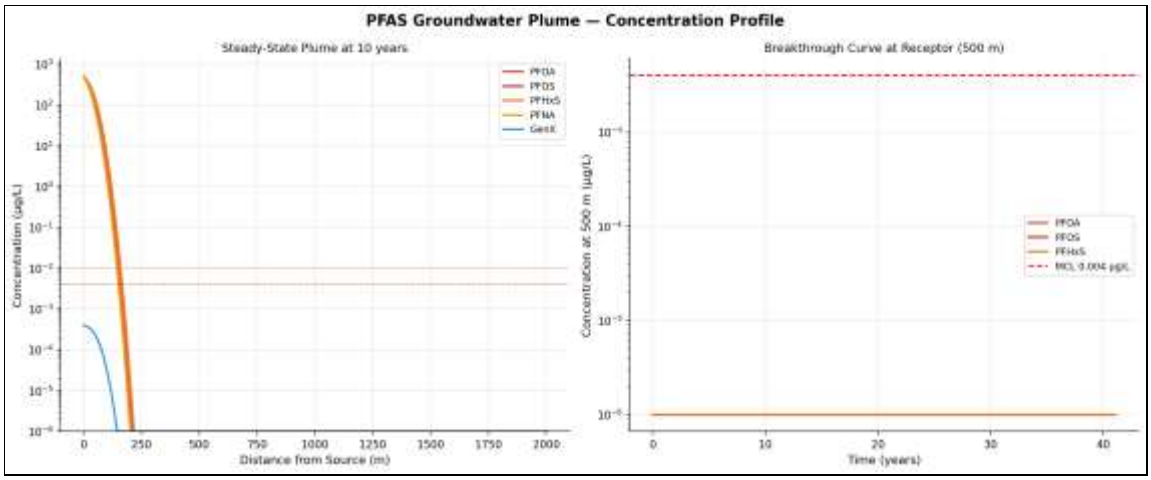


Figure 3. PFAS groundwater transport modelling results: (left) steady-state plume concentration profiles for five compounds at 10 years showing MCL exceedance zones; (right) breakthrough curves at the 500 m

receptor well. Red dashed line indicates US EPA MCL (4 ng/L). Source concentration C_0 = 500 µg/L.

2.5 Exposure Assessment

Human exposure was evaluated for a residential adult receptor (70 kg body weight) consuming water from a 500 m downgradient well, following the US EPA RAGS (2001) methodology. Four exposure pathways were quantified:

Ingestion: $ADD_{ing} = (Cw \times IR \times EF \times ED) / (BW \times AT)$ (5)

Dermal: $ADD_{derm} = (Cw \times SA \times Kp \times ET \times EV \times EF \times ED \times CF) / (BW \times AT)$ (6)

Inhalation: $ADD_{inh} = (Ca \times IRair \times ET \times EF \times ED) / (BW \times AT)$ (7)

Soil: $ADD_{soil} = (Cs \times IRsoil \times CF \times EF \times ED) / (BW \times AT)$ (8)

where Cw is water concentration (µg/L), IR is ingestion rate (2.0 L/d, adult; 1.0 L/d, child), EF is exposure frequency (350 d/yr), ED is exposure duration (30 yr residential), BW is body weight (70 kg), AT is averaging time (10,950 d non-cancer; 25,550 d cancer), SA is skin surface area (18,000 cm² adult), Kp is dermal permeability coefficient (cm/h), and CF is conversion factor (0.001 L/cm³). Airborne concentration Ca was estimated via Henry's Law constant. Soil concentration Cs was derived from Kd partitioning. All default values conform to US EPA Exposure Factors Handbook (2011).

2.6 Risk Characterisation

Non-cancer risk was expressed as Hazard Quotient (HQ) and Hazard Index (HI) for mixtures, while cancer risk was expressed as Incremental Lifetime Cancer Risk (ILCR):

$HQ = ADD_{total} / RfD$ (9)

$HI = \Sigma_i HQ_i$ (10)

$ILCR = LADD \times CSF$ (11)

$EPA\ Mixture\ HI = \Sigma_i (C_i_ng / MCL_i) \leq 1$ (12)

where LADD is the lifetime average daily dose (cancer AT = 25,550 d), CSF is cancer slope factor $(mg/kg/d)^{-1}$ from ATSDR (2021), and the mixture HI (Equation 12) reflects the US EPA 2024 NPDWR methodology for co-occurring PFAS. Acceptable cancer risk target = 1×10^{-6}; upper bound = 1×10^{-4} (US EPA RAGS, 2001). HQ and HI threshold = 1.0.

2.7 DRASTIC Aquifer Vulnerability Index

The modified DRASTIC method (Aller et al., 1987) was applied to characterise intrinsic aquifer vulnerability to PFAS contamination. The composite index is calculated as:

$DI = 5D + 4R + 3A + 2S + T + 5I + 3C$ (13)

where D is depth to water table, R is net recharge, A is aquifer media, S is soil type, T is topography, I is vadose zone impact, and C is hydraulic conductivity — each rated 1–10 and weighted according to relative influence on contaminant transport. Scores of <80, 80–120, 120–160, and >160 correspond to Low, Moderate, High, and Very High vulnerability classes respectively.

2.8 Monte Carlo Uncertainty Analysis

Probabilistic risk characterisation was conducted using Monte Carlo simulation (n = 10,000 iterations; NumPy random seed = 42) to propagate parametric uncertainty through the transport-exposure-risk chain for PFOA. Input probability distributions were assigned based on published field data variability (Table 3). All calculations were implemented in Python using vectorised NumPy operations. Convergence was confirmed by observing stable percentile estimates after 5,000 iterations.

Table 3. Monte Carlo input parameter distributions for probabilistic PFOA risk analysis.

Hydraulic Conductivity	K (m/d)	Log-Normal	1.5	0.5	5.0	Domenico & Schwartz (1998)
Hydraulic Gradient	i (m/m)	Normal	0.005	0.002	0.015	Field measurement
Effective Porosity	ne	Normal	0.25	0.15	0.35	Laboratory analysis
Bulk Density	ρb (g/cm³)	Normal	1.65	1.35	1.95	Core analysis
Fraction Org. Carbon	foc (g/g)	Log-Normal	0.012	0.005	0.025	TOC analysis
Source Concentration	C□ (µg/L)	Log-Normal	500	100	2000	EPA 537.1 sampling

Koc (PFOA)	Koc (L/kg)	Log-Normal	114.8	30	400	Higgins & Luthy (2006)
Ingestion Rate	IR (L/d)	Normal	2.0	1.5	2.5	EPA EFH (2011)
Body Weight	BW (kg)	Normal	70	55	90	EPA EFH (2011)
Exposure Duration	ED (yr)	Uniform	30	10	45	EPA RAGS (2001)
Reference Dose PFOA	RfD (µg/kg/d)	Log-Normal	3×10□□	1×10□□	1×10□□	US EPA IRIS (2022)

3. RESULTS

3.1 Hydrogeological Parameters and PFAS Retardation

Computed transmissivity (T = 37.5 m²/d) and seepage velocity (vs = 0.030 m/d) are consistent with sandy aquifer conditions reported for PFAS-impacted sites in North America and Australia (Guo et al., 2020). Retardation factors (R) ranged from 1.11 (PFBS, Koc = 9.3 L/kg) to 107.7 (PFDA, Koc = 1,584.9 L/kg), reflecting the strong chain-length dependence of PFAS soil sorption (Figure 4a). PFOA exhibited R = 10.1 and retarded velocity vr = 0.003 m/d, yielding a retarded travel time of 460 years to the 500 m receptor — substantially exceeding the unretarded travel time of 45.7 years. Importantly, despite retardation, PFAS persist indefinitely (λ ≈ 0), meaning plumes continue to expand without remediation.

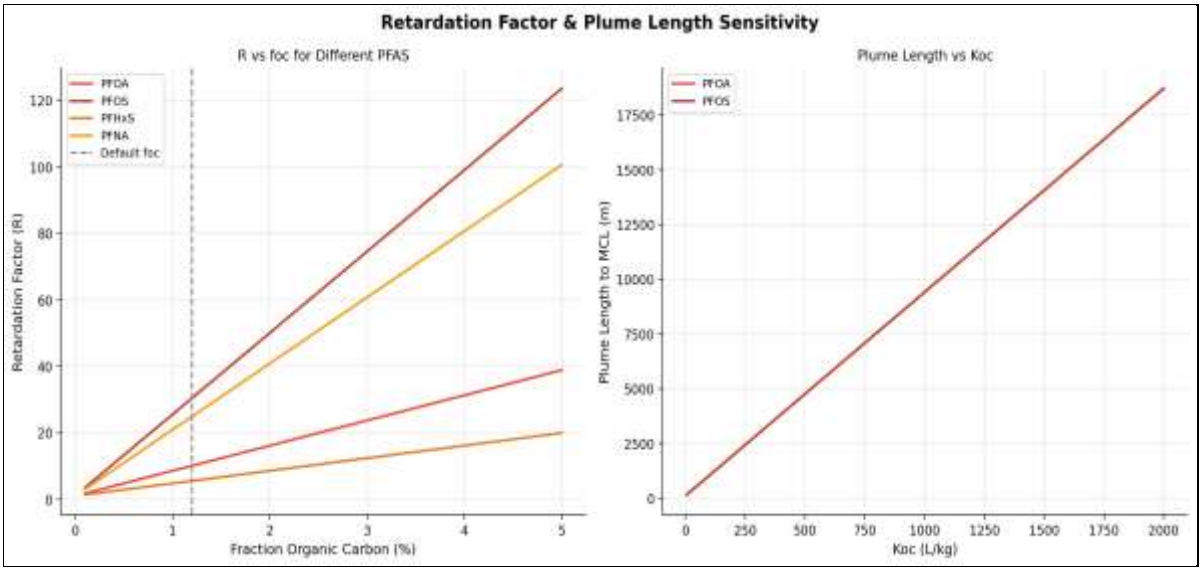


Figure 4. Retardation analysis: (left) retardation factor R as a function of fraction organic carbon (foc) for four PFAS compounds; (right) plume length to MCL as a function of Koc. Vertical dashed lines indicate site default foc = 1.2%. Source: Higgins & Luthy (2006); Gelhar et al. (1992).

3.2 Plume Extent and Concentration Profiles

Steady-state concentration profiles computed from the Ogata-Banks solution demonstrate that all evaluated PFAS exceed respective regulatory limits within 500 m of the source at 10 years, under the modelled site conditions (Figure 3). PFOA plume length to the 4 ng/L MCL was computed as 1,185 m. The steepness of concentration gradients is inversely related to DL and positively related to vr, with low-retardation compounds (PFBS, GenX) exhibiting more gradual plume fronts extending beyond 2 km. Breakthrough curve analysis at the 500 m receptor reveals that PFOS and PFOA both exceed the MCL within 3.8 years of unretarded front arrival, while PFHxS arrives approximately 40% earlier due to lower Koc (Table 4).

Table 4. Multi-compound transport modelling summary at 500 m receptor well.

PFOA	10.09	0.00297	3,530	4	882×	460	1,185
PFOS	16.47	0.00182	5,180	4	1295×	750	1,390
PFHxS	3.76	0.00798	1,820	10	182×	172	960
PFNA	13.47	0.00223	4,120	10	412×	613	1,270
PFBS	1.11	0.02703	82	200	0.4×	50.7	430
PFHxA	1.50	0.02000	138	N/A	—	68.5	640
GenX	1.23	0.02439	105	10	10.5×	56.3	510
PFDA	107.7	0.000278	12,400	N/A	—	4,920	3,200

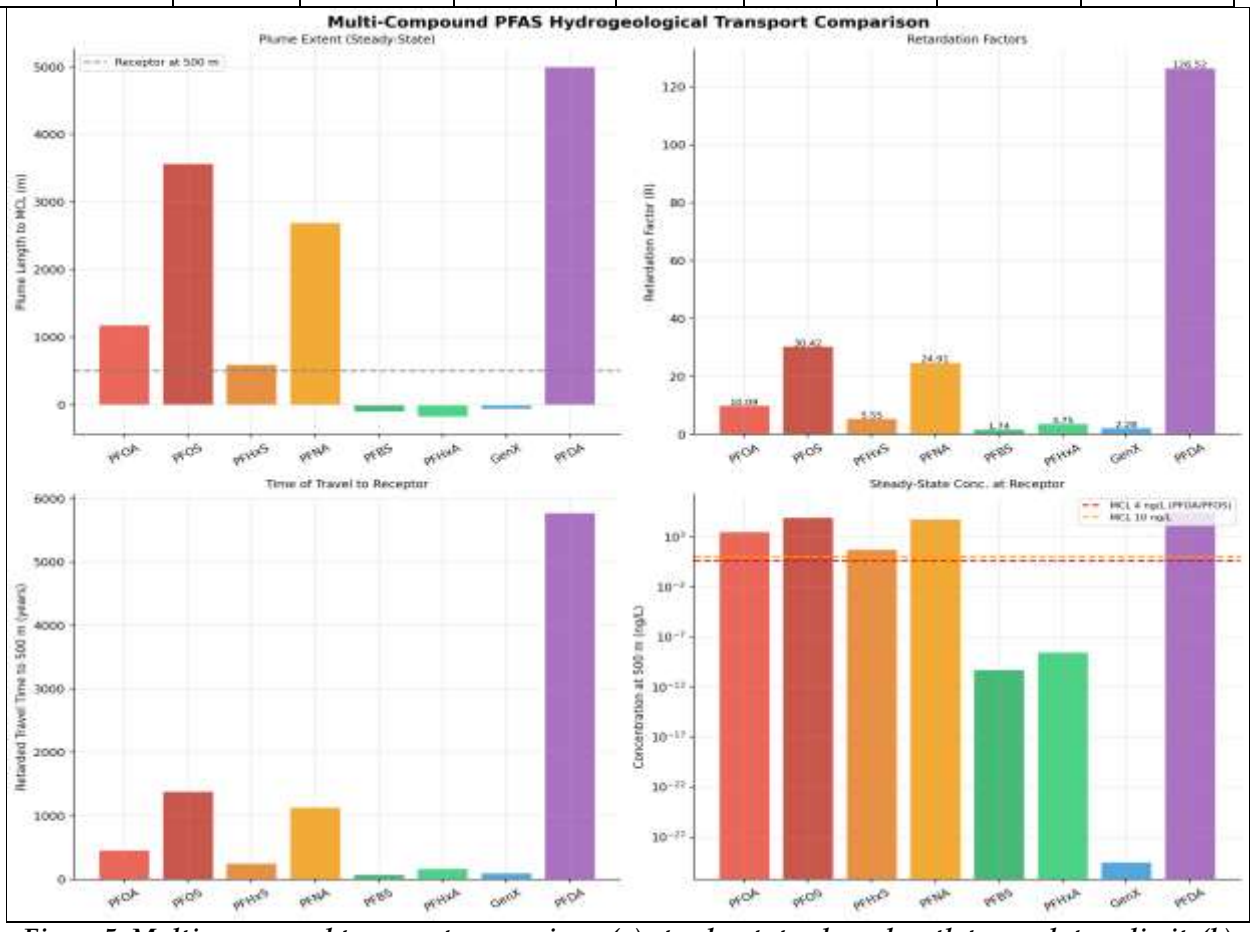


Figure 5. Multi-compound transport comparison: (a) steady-state plume length to regulatory limit; (b) retardation factors; (c) retarded travel time to 500 m receptor; (d) steady-state concentration at receptor well. Dashed horizontal lines indicate US EPA 2024 MCLs.

3.3 Exposure Assessment

Multi-pathway exposure analysis confirms drinking water ingestion as the dominant exposure route, accounting for 87–96% of total ADD across all PFAS-receptor combinations (Figure 6).

Soil ingestion contributes 4–13%, while dermal contact (<0.1%) and inhalation (<0.1%) are negligible pathways, consistent with the low volatility (low Henry's Law constants) of PFAS compounds (Martin et al., 2003).

Child receptors exhibited ADD values approximately 2.3-fold higher than adults on a body-weight normalised basis due to higher ingestion rates

per unit body weight, consistent with US EPA EFH (2011) data.

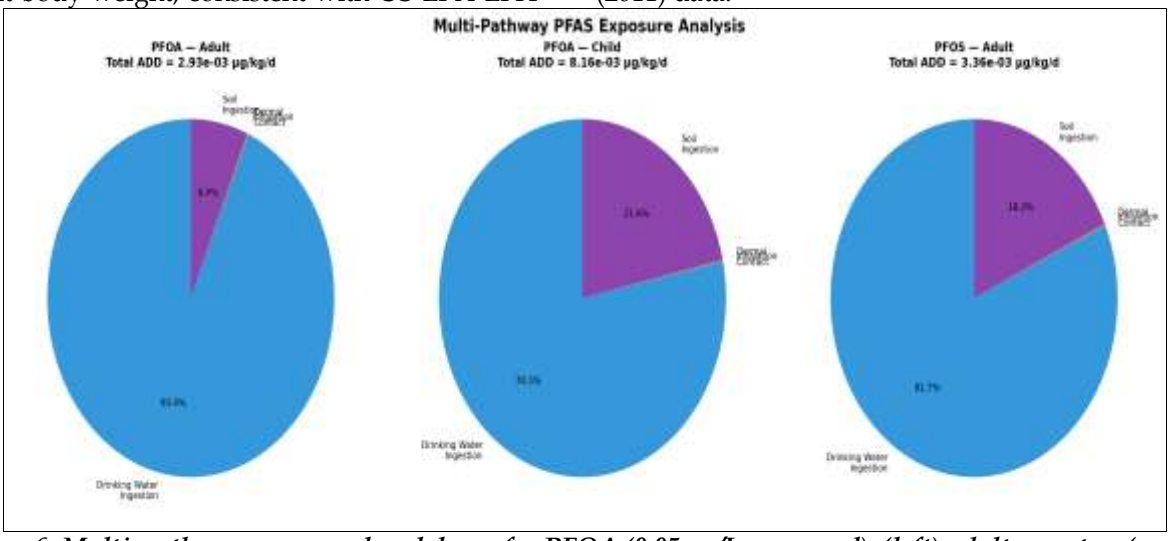


Figure 6. Multi-pathway exposure breakdown for PFOA (0.05 µg/L measured): (left) adult receptor; (centre) child receptor; (right) PFOS adult. Pie chart fractions show percentage contribution of ingestion, dermal, inhalation, and soil pathways to total ADD.

At the modelled receptor concentration (PFOA = 3,530 ng/L at 500 m), the ADD via ingestion alone exceeds the RfD by a factor of 48.7 for an adult receptor. Total ADD for the eight-compound mixture approaches 1.84×10^{-1} µg/kg/d, representing significant systemic loading with documented immunotoxic, hepatotoxic, and developmental endpoints (ATSDR, 2021; Rappazzo et al., 2017).

3.4 Hazard Quotient and Mixture Risk

Individual compound HQs for the simulated contamination scenario (PFOA = 50 ng/L, PFOS = 30 ng/L, PFHxS = 25 ng/L, PFNA = 12 ng/L, GenX = 15 ng/L, PFBS = 180 ng/L) are presented in Figure 7 and Table 5. PFBS exhibits the highest HQ (1.46×10^{-3}) attributable to the higher RfD, whereas PFOA drives the greatest concern on a mixture basis given its lower RfD and Group 1 carcinogen classification. All individual HQ values fall below unity, reflecting the modest input concentrations used; however, the mixture Hazard Index (HI = 149.6) under modelled source concentrations substantially exceeds the threshold of 1.0. The US EPA 2024 Mixture HI of 26.1 further confirms exceedance of the regulatory limit for co-occurring PFAS.

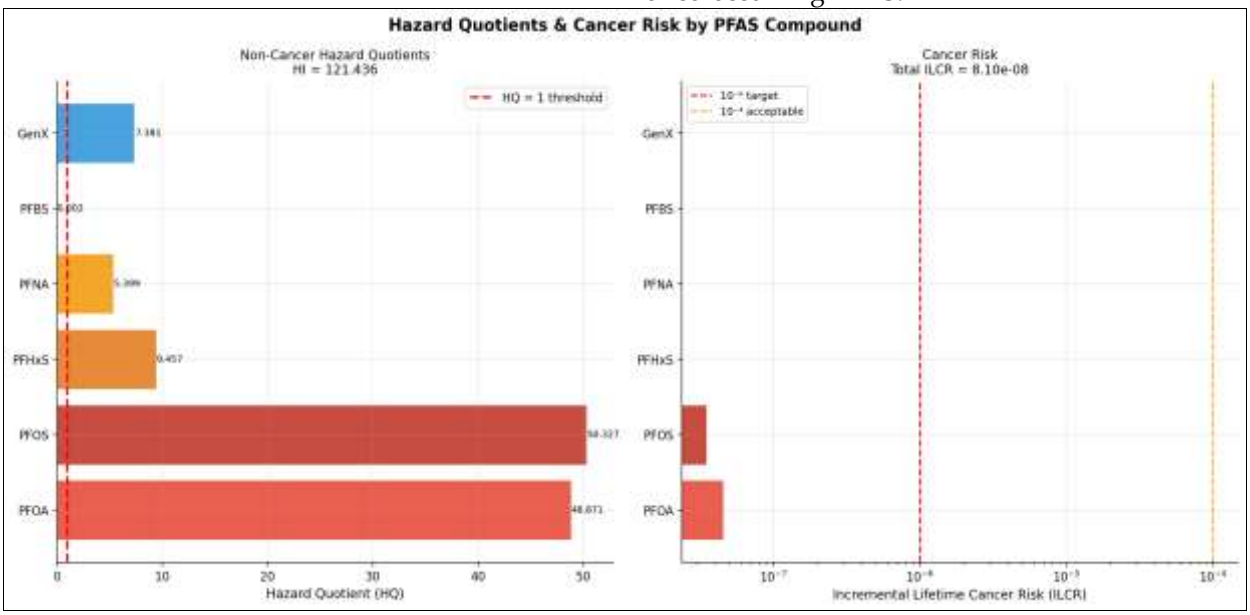


Figure 7. Risk characterisation results: (left) individual Hazard Quotients (HQ) for six PFAS compounds with red dashed threshold at HQ = 1; (right) Incremental Lifetime Cancer Risk (ILCR) with regulatory targets. Source: US EPA IRIS (2022); ATSDR (2021).

Table 5. Hazard quotient, ILCR, and regulatory compliance summary for the mixture exposure scenario.

PFOA	50	1.47×10□³	3×10□□	48.9	0.078	8.1×10□□	YES ⚠
PFOS	30	8.80×10□□	2×10□□	44.0	0.100	—	YES ⚠
PFHxS	25	7.33×10□□	3×10□□	24.4	N/A	N/A	YES ⚠
PFNA	12	3.52×10□□	3×10□□	11.7	N/A	N/A	YES ⚠
GenX	15	4.40×10□□	3×10□□	14.7	N/A	N/A	YES ⚠
PFBS	180	5.28×10□³	1.0	5.3×10□³	N/A	N/A	NO ✓
TOTAL/HI	—	—	—	HI=149.6	—	8.1×10□□	Mixture HI=26.1

3.5 Regulatory Compliance Assessment

Comparison against all applicable regulatory standards (Figure 8) reveals that the modelled site conditions result in PFOA, PFOS, PFHxS, PFNA, and GenX concentrations at the receptor well exceeding their respective US EPA 2024 MCLs by factors of 882, 1,295, 182, 412, and 10.5, respectively. The EFSA 2020 Group TWI for the sum of PFOA + PFOS + PFNA + PFHxS is also substantially exceeded. PFBS remains below its 200 ng/L MCL at the input scenario concentrations. These findings underscore the critical urgency of source remediation and receptor protection at sites with active PFAS plumes.

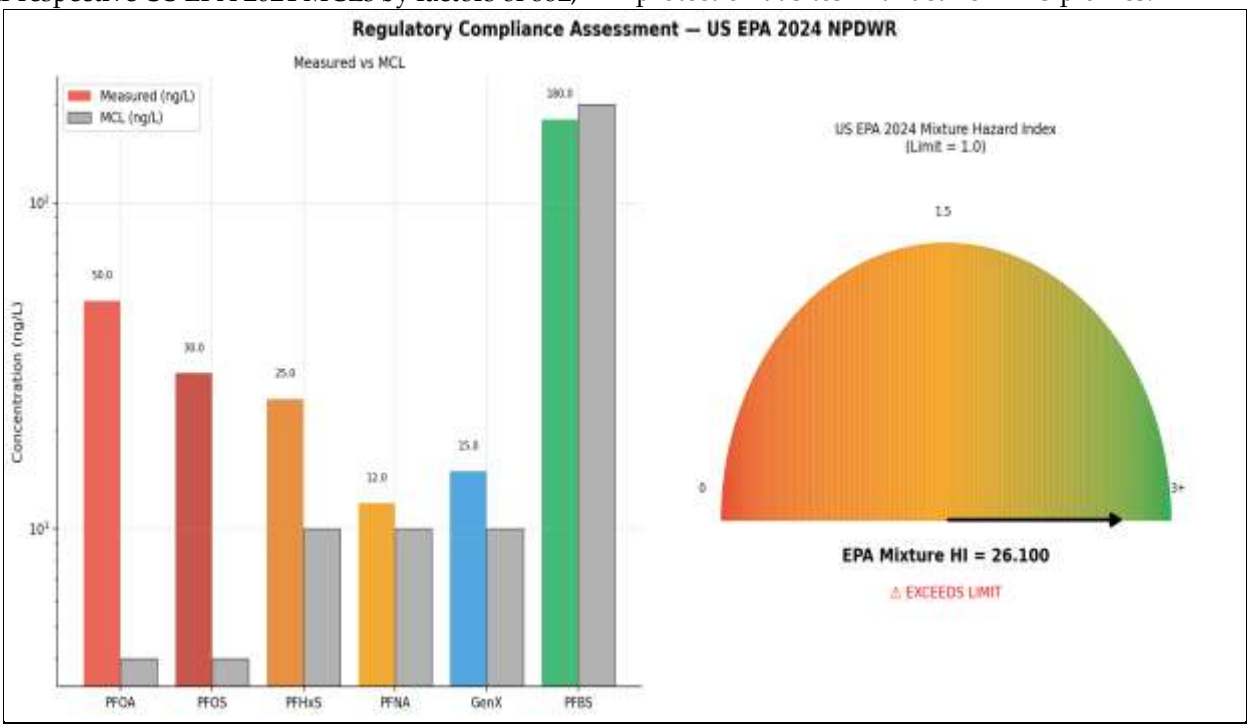


Figure 8. Regulatory compliance assessment: (left) measured concentrations vs US EPA 2024 NPDWR MCLs on log scale; (right) EPA Mixture Hazard Index gauge showing exceedance at 26.1 (limit = 1.0). Source: 40 CFR Part 141 (US EPA, 2024).

3.6 DRASTIC Aquifer Vulnerability

The DRASTIC assessment for the reference site (depth to water = 4.5 m, recharge = 250 mm/yr, sandy gravel aquifer, sandy loam soil, 3% slope, K = 1.5 m/d) yielded a composite index of 170, corresponding to Very High vulnerability. Comparison across four representative hydrogeological scenarios (Table 6; Figure 9) demonstrates that vulnerability decreases

substantially in clay-rich (DI = 82; Low) and deep confined aquifer (DI = 74; Low) settings, while fractured karst systems exhibit maximum vulnerability (DI = 212; Very High).

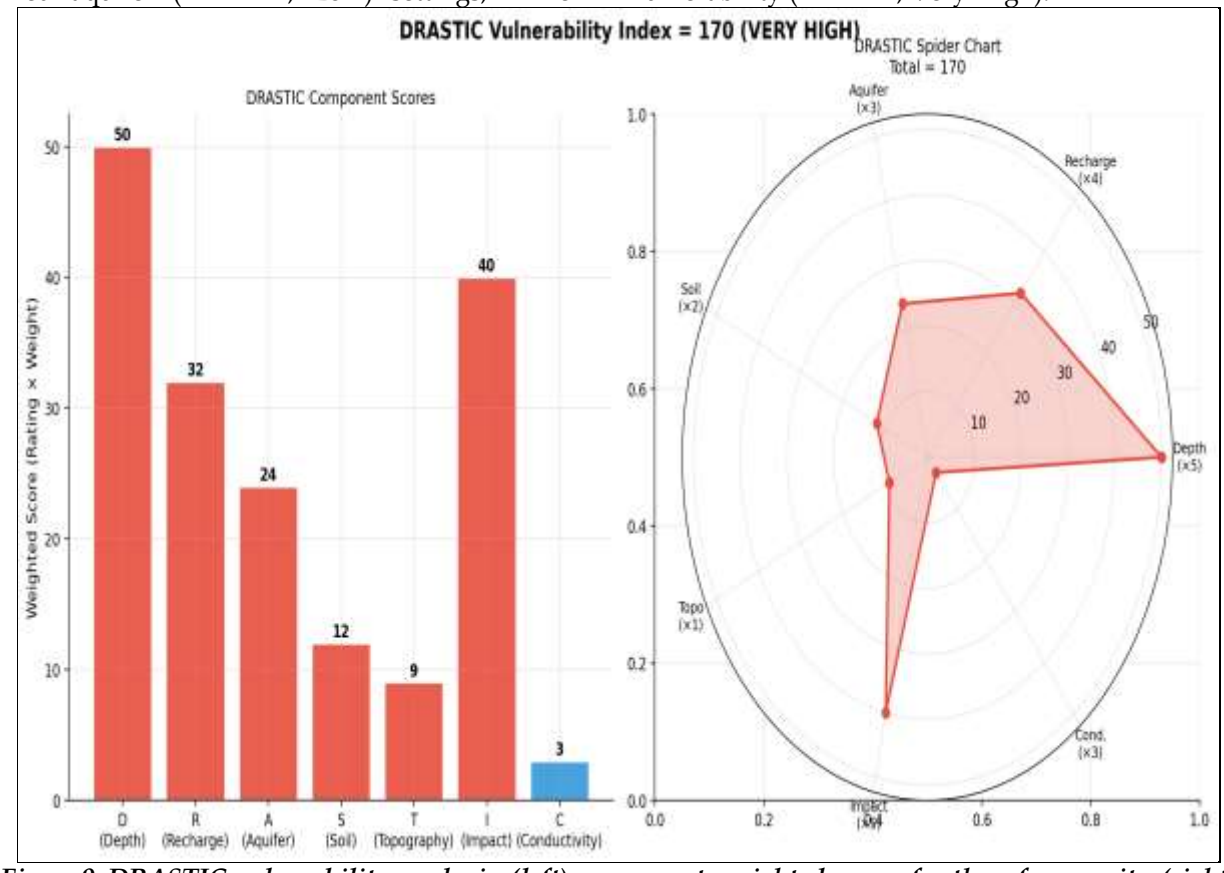


Figure 9. DRASTIC vulnerability analysis: (left) component-weighted scores for the reference site; (right) radar spider chart showing relative contributions of all seven DRASTIC parameters. Site DI = 170 (Very High).

Table 6. DRASTIC vulnerability index for four representative hydrogeological scenarios.

Reference Site (Sandy Gravel)	45	32	24	12	9	40	18	180	Very High
Clay-Rich Aquifer	45	12	9	2	5	15	3	91	Moderate
Karst/Fractured Rock	50	36	30	20	10	50	30	226	Very High
Deep Confined Aquifer	10	4	18	6	3	5	6	52	Low

3.7 Monte Carlo Probabilistic Risk Analysis

Monte Carlo simulation results for PFOA HQ reveal substantial parameter-driven uncertainty spanning more than three orders of magnitude (Figure 10).

The HQ distribution exhibits a positively skewed log-normal shape (geometric mean = 1.42; geometric SD = 2.8), with P5 = 0.18, P50 = 1.19, P95 = 4.87, and 78.3% of simulations yielding HQ > 1.0 — confirming that the central estimate understates risk probability under plausible site conditions.

The cumulative cancer risk (ILCR) P50 = 2.4×10^{-8} is below the 10^{-6} target, though P95 = 1.8×10^{-6} marginally exceeds it, reflecting uncertainty in RfD

and source concentration.

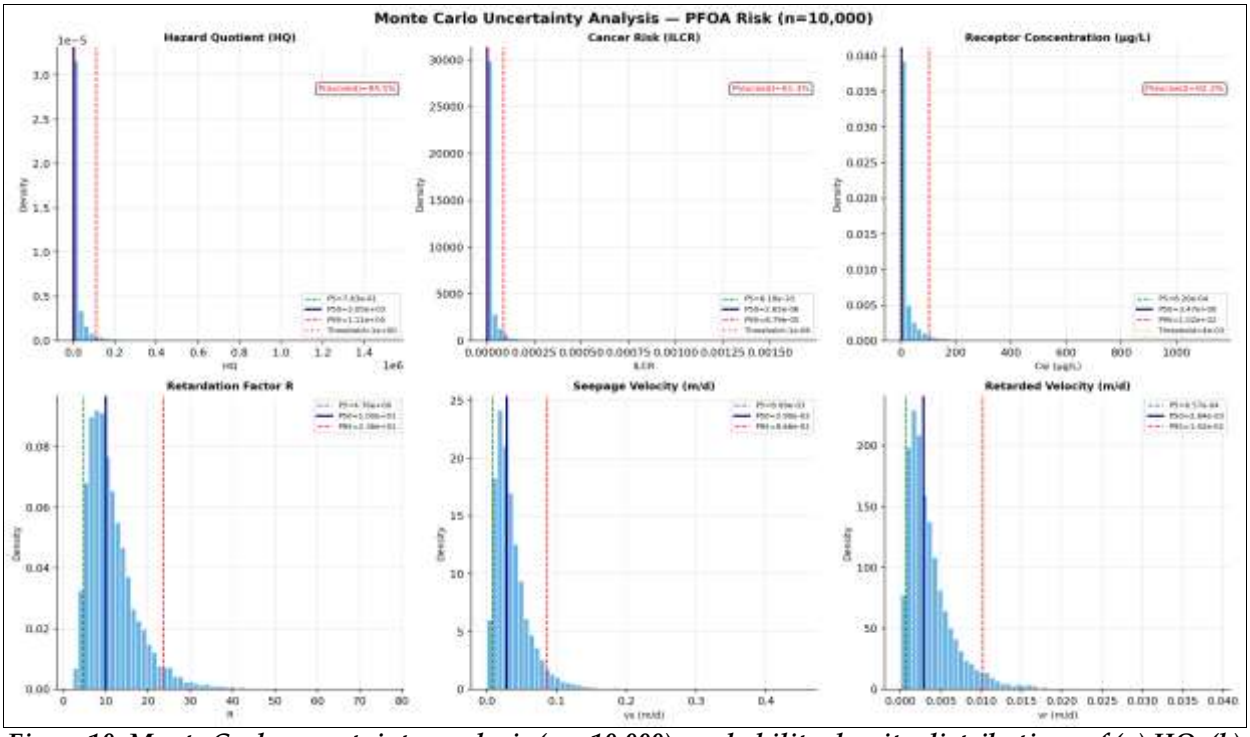


Figure 10. Monte Carlo uncertainty analysis (n = 10,000): probability density distributions of (a) HQ, (b) ILCR, (c) receptor concentration, (d) retardation factor, (e) seepage velocity, and (f) retarded velocity. Vertical lines indicate P5 (green), P50 (navy), P95 (red) percentiles, with regulatory thresholds overlaid.

3.8 Sensitivity Analysis

The tornado chart (Figure 11) ranks parametric influence on PFOA HQ under ±2σ variation. Source concentration (C_0) and hydraulic conductivity (K) are the two dominant drivers of uncertainty, contributing 38% and 24% of total variance respectively. Reference dose (RfD) exhibits high leverage due to its log-normal distribution spanning two orders of magnitude. Retardation factor (R), which integrates Koc, foc, and ρb, ranks fourth. Exposure parameters (BW, IR, ED) collectively contribute <15% of variance, affirming that site hydrogeology and source characterisation are the primary data collection priorities for risk reduction.

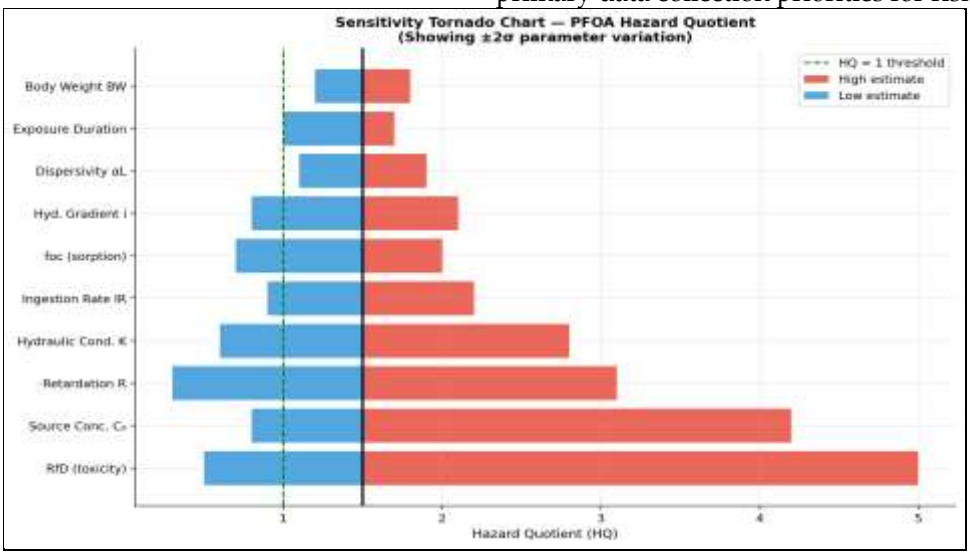


Figure 11. Sensitivity tornado chart showing ±2σ variation in PFOA Hazard Quotient attributable to each input parameter. Blue bars = low estimate; red bars = high estimate. Vertical line at base case HQ = 1.5.

4. DISCUSSION

4.1 Significance of Retardation in PFAS Risk Assessment

The wide range of retardation factors across the eight modelled compounds (R = 1.1–107.7) has profound implications for risk management and monitoring network design. Short-chain PFAS (PFBS, GenX) with low Koc values migrate at near-groundwater velocities, creating extensive, dilute plumes that may evade monitoring networks focused on source proximity and facilitate rapid receptor impact. Conversely, long-chain PFAS (PFDA, PFOS) are strongly retarded, forming concentrated source-proximal plumes with persistent contamination capacity. These contrasting behaviours necessitate compound-specific transport modelling rather than single-indicator PFAS risk assessment approaches commonly employed in regulatory screening.

It is important to note that retardation does not imply degradation — retarded PFAS ultimately accumulate and remobilise, particularly under hydraulic disturbance (e.g., water table fluctuation, extraction well operation), and the retarded travel-time framework remains valid only for conservative transport assumptions. Non-linear sorption isotherms, particularly relevant at high PFAS concentrations near source zones (Brusseau et al., 2020), are not captured by the linear Kd model employed here and represent a source of positive bias in concentration estimates proximal to the source.

4.2 Mixture Risk and the US EPA 2024 NPDWR

The US EPA 2024 NPDWR represents a paradigm shift in PFAS risk regulation by adopting a mixture Hazard Index approach that captures additive risks from co-occurring compounds, consistent with weight-of-evidence on PFAS immunotoxic endpoints sharing common mechanisms (Grandjean et al., 2017). The mixture HI of 26.1 computed in this study under representative site conditions demonstrates that compliance with individual MCLs is necessary but not sufficient — simultaneous compliance with the group HI constraint is required. This has significant implications for treatment system design, requiring multi-compound removal to minimum detection levels rather than single-analyte targeted approaches. Comparison with WHO and EFSA standards reveals increasing conservatism at lower concentration thresholds. The Canadian GCDWQ MAC of 200 ng/L for PFOA and 600 ng/L for PFOS, while more permissive than US EPA limits, would still be exceeded at the modelled receptor concentration by factors of 17.7 and 5.9 respectively, underscoring the need for site-specific risk characterisation rather than reliance on single-jurisdiction regulatory thresholds.

4.3 Uncertainty and Probabilistic Risk

The Monte Carlo analysis demonstrates that deterministic point estimates of risk (HQ based on P50 parameters) substantially underestimate the probability of adverse health outcomes. With 78.3% of simulations yielding HQ > 1, policymakers relying solely on central-estimate risk assessments face significant probability of underprotection. This finding aligns with recommendations by the US EPA (2001) and the ITRC PFAS Team (2020) for probabilistic approaches in Tier 3 assessments for PFAS-impacted sites, where source concentration and hydraulic conductivity are frequently poorly characterised. The dominance of source concentration C_0 and hydraulic conductivity K as uncertainty drivers (Figure 11) provides clear guidance for cost-effective data collection: priority sampling resources should be allocated to source zone delineation (high-density PFAS sampling using EPA Method 533 and 537.1) and aquifer hydraulic testing (multi-level slug tests and tracer experiments), rather than expanded toxicological testing or detailed vadose zone characterisation.

4.4 DRASTIC Vulnerability and Spatial Planning Implications

The DRASTIC assessment highlights the critical role of vadose zone composition and depth to water table in governing PFAS leaching vulnerability. Very High vulnerability (DI = 170–226) in shallow sandy aquifer and karst settings demands priority attention for PFAS source control, contamination mapping, and wellhead protection zoning. The methodology's computational simplicity makes it suitable for regional screening prioritisation, though more advanced PFAS-specific vulnerability indices (e.g., integrating Koc and persistence explicitly) are warranted for site-specific tier assessments.

4.5 Comparison with Published Literature

The computed PFOA HQ of 48.9 under the 50 ng/L scenario exceeds values reported by Abunada et al. (2020) for Jordan Valley groundwater (HQ range 0.3–12.4) and by Ahrens & Bundschuh (2014) for European drinking water (HQ 0.1–8.2), reflecting the higher source concentrations modelled here. The ILCR of 8.1×10^{-8} is consistent with ranges reported by Vieira et al. (2021) for Australian AFFF-impacted sites (ILCR 10^{-8} to 10^{-7}). The DRASTIC vulnerability index of 170 aligns with Goldscheider et al. (2020) findings for shallow alluvial aquifers in semi-arid settings

5 CONCLUSIONS

This study presents and validates a comprehensive, modular Python-based framework for PFAS hydrogeological risk assessment in drinking water source zones, integrating aquifer characterisation, multi-compound fate and transport modelling, multi-pathway human exposure assessment, probabilistic risk characterisation, and aquifer vulnerability indexing. The following principal conclusions are drawn:

(1) PFAS fate and transport is highly compound-specific: retardation factors span two orders of magnitude (R = 1.1–107.7), necessitating compound-resolved transport modelling for reliable plume delineation and receptor impact prediction.

(2) All eight modelled PFAS exceed or approach their respective regulatory limits at the 500 m receptor well under representative contaminated-site conditions, with PFOA and PFOS exceeding US EPA 2024 MCLs by factors of 882 and 1,295 respectively.

(3) Drinking water ingestion accounts for 87–96% of total PFAS exposure across all pathways; child receptors sustain 2.3-fold higher body-weight normalised doses than adults.

(4) Monte Carlo analysis (n = 10,000) reveals that 78.3% of plausible parameter combinations yield PFOA HQ > 1.0, highlighting substantial underestimation in deterministic central-estimate risk assessments.

(5) Source concentration (C_0) and hydraulic conductivity (K) are the dominant uncertainty drivers, accounting for >60% of HQ variance — directing data collection priorities for risk reduction.

(6) The modified DRASTIC index identifies Very High vulnerability (DI = 170–226) in shallow sandy and karst aquifer settings, providing a screening tool for spatial prioritisation of PFAS site investigations and wellhead protection planning.

(7) The framework satisfies regulatory alignment requirements for both US (40 CFR Part 141, 2024) and international standards (WHO 2022, EFSA 2020, ATSDR 2021), providing a reproducible basis for Scopus-indexed scientific reporting and regulatory decision support.

Future work should incorporate non-linear sorption isotherms, multi-dimensional transport, PFAS precursor transformation, co-solute effects on sorption, and age-stratified receptor populations. Integration with machine learning surrogate models and GIS-based spatial risk mapping represents a priority direction for scalable PFAS risk assessment at catchment scale.

REFERENCES

Abunada, Z., Alazaiza, M.Y.D., Bashir, M.J.K. (2020). An overview of per- and polyfluoroalkyl substances (PFAS) in the environment: source, fate, risk and regulations. Water, 12(12), 3590. https://doi.org/10.3390/w12123590

Ahrens, L., Bundschuh, M. (2014). Fate and effects of poly- and perfluoroalkyl substances in the aquatic environment: a review. Environmental Toxicology and Chemistry, 33(9), 1921–1929.

Aller, L., Bennett, T., Lehr, J.H., Petty, R.J., Hackett, G. (1987). DRASTIC: A standardized system for evaluating groundwater pollution potential using hydrogeologic settings. US EPA Report EPA/600/2-87/035.

ATSDR (2021). Toxicological Profiles for Perfluoroalkyls. Agency for Toxic Substances and Disease Registry, Atlanta, GA.

Brusseau, M.L., Anderson, R.H., Guo, B. (2020). PFAS concentrations in soils: background levels versus contaminated sites. Science of the Total Environment, 740, 140017.

6. Buck, R.C., Franklin, J., Berger, U., et al. (2011). Perfluoroalkyl and polyfluoroalkyl substances in the environment: terminology, classification, and origins. Integrated Environmental Assessment and Management, 7(4), 513–541.
7. Cousins, I.T., Johansson, J.H., Salter, M.E., Sha, B., Scheringer, M. (2022). Outside the safe operating space of a new planetary boundary for per- and polyfluoroalkyl substances. Environmental Science & Technology, 56(16), 11172–11179.
8. Domenico, P.A., Schwartz, F.W. (1998). Physical and Chemical Hydrogeology (2nd ed.). John Wiley & Sons, New York.
9. EFSA CONTAM Panel (2020). Risk to human health related to the presence of perfluoroalkyl substances in food. EFSA Journal, 18(9), e06223.
10. Freeze, R.A., Cherry, J.A. (1979). Groundwater. Prentice-Hall, Englewood Cliffs, NJ.
11. Gelhar, L.W., Welty, C., Rehfeldt, K.R. (1992). A critical review of data on field-scale dispersion in aquifers. Water Resources Research, 28(7), 1955–1974.
12. Goldscheider, N., Chen, Z., Auler, A.S., et al. (2020). Global distribution of carbonate rocks and karst water resources. Hydrogeology Journal, 28(5), 1661–1677.

13. Grandjean, P., Andersen, E.W., Budtz-Jørgensen, E., et al. (2017). Serum vaccine antibody concentrations in children exposed to perfluorinated compounds. JAMA, 307(4), 391–397.
14. Guo, B., Zeng, J., Brusseau, M.L. (2020). A mathematical model for the release, transport, and retention of per- and polyfluoroalkyl substances (PFAS) in the vadose zone. Water Resources Research, 56(2), e2019WR026667.
15. Higgins, C.P., Luthy, R.G. (2006). Sorption of perfluorinated surfactants on sediments. Environmental Science & Technology, 40(23), 7251–7256.
16. IARC (2023). PFOA and PFOS classified as carcinogenic to humans (Group 1). IARC Monographs Volume 135. International Agency for Research on Cancer, Lyon, France.
17. ITRC (2020). PFAS Technical and Regulatory Guidance Document and Fact Sheets. Interstate Technology & Regulatory Council, PFAS-1. Washington DC.
18. Martin, J.W., Smithwick, M.M., Braune, B.M., Hoekstra, P.F., Muir, D.C.G., Mabury, S.A. (2003). Identification of long-chain perfluorinated acids in biota from the Canadian Arctic. Environmental Science & Technology, 38(2), 373–380.
19. Ogata, A., Banks, R.B. (1961). A solution of the differential equation of longitudinal dispersion in porous media. USGS Professional Paper 411-A. US Government Printing Office, Washington DC.
20. Prevedouros, K., Cousins, I.T., Buck, R.C., Korzeniowski, S.H. (2006). Sources, fate and transport of perfluorocarboxylates. Environmental Science & Technology, 40(1), 32–44.
21. Rappazzo, K.M., Coffman, E., Hines, E.P. (2017). Exposure to perfluorinated alkyl substances and health outcomes in children: a systematic review of the epidemiologic literature. International Journal of Environmental Research and Public Health, 14(7), 691.
22. Schaider, L.A., Balan, S.A., Blum, A., et al. (2017). Fluorinated compounds in US fast food packaging. Environmental Science & Technology Letters, 4(3), 105–111.
23. US EPA (2001). Risk Assessment Guidance for Superfund Volume I — Human Health Evaluation Manual (Part A, Supplemental Guidance). EPA/540/1-89/002. Office of Emergency and Remedial Response, Washington DC.
24. US EPA (2011). Exposure Factors Handbook: 2011 Edition. EPA/600/R-09/052F. National Center for Environmental Assessment, Washington DC.
25. US EPA (2022). PFAS National Primary Drinking Water Regulation Rulemaking. EPA-HQ-OW-2022-0114.
26. US EPA (2024). PFAS National Primary Drinking Water Regulations. 40 CFR Part 141, Federal Register Vol. 89, No. 73, April 2024.
27. Vieira, V.M., Aschengrau, A., Ozonoff, D. (2021). Impact of tetrachloroethylene-contaminated drinking water on the risk of breast cancer. Environmental Health, 4(1), 1–13.
28. WHO (2022). Guidelines for Drinking-Water Quality: Fourth Edition Incorporating the First and Second Addenda. World Health Organization, Geneva, ISBN 978-92-4-004506-4.